Doppler Influence on Waveform Orthogonality in 79GHz MIMO Phase-Coded Automotive Radar

Overdevest, Jeroen; Jansen, Feike; Uysal, Faruk; Yarovoy, Alexander

DOI
10.1109/TVT.2019.2951632

Publication date
2020

Document Version
Final published version

Published in
IEEE Transactions on Vehicular Technology

Doppler Influence on Waveform Orthogonality in 79 GHz MIMO Phase-Coded Automotive Radar

Jeroen Overdevest, Feike Jansen, Faruk Uysal, *Senior Member, IEEE*, and Alexander Yarovoy, *Fellow, IEEE*

***Abstract*—Utilization of phase-coded waveforms in automotive MIMO radars for short to medium range applications is studied. Performances of three most-promising binary code families (Gold, APAS and ZCZ sequences) are compared. Design trade-offs of practical implementation of phased-coded waveforms for MIMO radar are analyzed for the first time for a possible future System on Chip implementation. Orthogonality of the waveforms in case of moving targets is analyzed. The implications of the code properties for the Range-Doppler map, as well as the Range-Angular map, are pointed out. Doppler frequency shift impact on such performance indicators as the target peak power and range sidelobe levels in the range-Doppler plane, as well as the range and azimuth sidelobe behavior, and the angular error in the azimuthal plane have been comprehensively studied for the first time. It is shown that the time-staggered transmit scheme with autocorrelation properties only (while introducing azimuthal errors) results in improved performance compared to code division multiplexing with auto- and cross-correlation properties.**

***Index Terms*—Automotive radar, PMCW, binary sequences, waveform orthogonality, Doppler influences.**

I. Introduction

AUTOMOTIVE radar plays a crucial role in the reduction of traffic casualties and the realization of autonomous driving due to its robustness and adverse weather tolerance. Frequency-Modulated Continuous Wave (FMCW) radars have matured over the last couple of years while more complex system architectures and enhanced DSP algorithms have become available. These designs feature MIMO architectures, which benefit over conventional radar systems in terms of increased detection probabilities by combining multiple channel outputs, estimation of azimuthal angular information, etc. [1]. Azimuthal angular resolution can be enhanced by increasing the number of transmit and/or receive antennas, which (by fixed distance between antennas) results in an increase of the antenna array aperture size [2], [3]. The demand for higher angular resolution and detection probability increase pushes towards further increase of MIMO transmit channel numbers [4], while the need of shorter measurement time requires the transition from sequential to simultaneous MIMO measurements with mutually orthogonal waveforms transmitted from different channels. Therefore, the need for transmit (quasi-) orthogonal waveforms is enormous in the MIMO radar field.

In FMCW MIMO systems, time-division multiple access (TDMA) or frequency-division multiple access (FDMA) has to be applied to realize simultaneous transmission and avoid cross-correlation among the transmitted waveforms. Recently, an alternative to FMCW modulation has gained attraction in the field of automotive radar, which is called Phase-Modulated Continuous Wave (PMCW) radar [5]–[9]. This modulation type is able to create multiple channel accesses by transmitting coded waveforms simultaneously, thus profiting of the full capacity.

A complete orthogonality study for PMCW radar systems has not been addressed in the currently available literature. In [10], [11], the performance of PMCW waveforms has been simulated using reflections from static targets. However, to get a more realistic view on the performance of the phase-modulated waveforms, analysis needs to be extended towards its main weakness: Doppler intolerance; and how this intolerance influences the orthogonality principles. In the application of automotive, we can address the range of velocities for which the performance of the radar should be attained. The intention of this paper is not to compensation for the Doppler distortions. Doppler compensation for BPSK PMCW has been investigated in the past, which resulted in several algorithms to alleviate its Doppler vulnerability, e.g. based on a recursive MMSE method [12] or multichannel correlators emulating for various Doppler shifts [13]. These would require tremendous computational powers, which currently does not fit industrial needs for a System on Chip solution.

In the search to promising code sets for PMCW radar, many code families have been explored in the past. Different classes of codes can be distinguished, ranging from binary sequences (Barker, M-sequence, Gold, Kasami [14], etc.), to complementary pairs (Golay [15]) and poly-phase codes [16] (Frank [17], P1-P2-P3-P4 codes [18]). Binary codes having other BPSK constellation than $\{0, \pi\}$ also exist, such as Golomb codes [19], but are not considered in this paper. Complementary codes, such as Golay codes, show very auspicious auto- and cross-correlation values; however, the sum of the autocorrelation is prone to Doppler sensitivities [20]. While Doppler tolerance improvement of Golay codes have been proposed in [21], its

Manuscript received June 24, 2019; accepted October 6, 2019. Date of publication November 5, 2019; date of current version January 15, 2020. The review of this article was coordinated by Dr. Sunwoo Kim. *(Corresponding author: Jeroen Overdevest.)*

J. Overdevest is with the NXP Semiconductors N.V., Eindhoven, The Netherlands, and also with Microwave Sensing, Systems and Signals (MS3) group, at Faculty of Electrical Engineering, Mathematics and Computer Science (EEMCS), Delft University of Technology, 2628 Delft, The Netherlands (e-mail: jeroen.overdevest@nxp.com).

F. Jansen is with the NXP Semiconductors N.V., Eindhoven, The Netherlands (e-mail: feike.jansen@nxp.com).

F. Uysal and A. Yarovoy are with the the Microwave Sensing, Systems and Signals (MS3) group, at Faculty of Electrical Engineering, Mathematics and Computer Science (EEMCS), Delft University of Technology, Delft, The Netherlands (e-mail: f.uysal@tudelft.nl; a.yarovoy@tudelft.nl).

Digital Object Identifier 10.1109/TVT.2019.2951632

application is limited by the relatively short realizable code lengths as well as small complementary sets. On the other hand, poly-phase codes show better Doppler resilience compared to binary and complementary sequences, but resembles discrete approximations of linear FM transmitted waveforms and thus have comparable performance to FMCW radars [22].

Impact of Doppler frequency shifts on orthogonality of binary sequences, as well as such performance indicators of the codes such as sidelobe level of target image in the Range-Doppler and Range-Azimuth planes, produced by a MIMO PMCW radar are analyzed in this paper for the first time. Furthermore, different code sets have different peculiarities from implementation in MIMO radar point of view. E.g., most of the codes contain unfavorable characteristics, in terms of either the possibilities in generating a desired code set size and/or code length, or performance. For example, the *prefered* m-sequences have good autocorrelation properties but its downsides are its relatively high cross-correlation values as well the highly limited realizable set size [14]. Thus, this paper also discusses the design trade offs in PMCW automotive radar which (as for our best knowledge) has never been discussed with such aspects before. As a result of this analysis, we point out the three most promising binary (or bi-phase) sequences: Gold, APAS and ZCZ sequences for automotive radar applications. As performance of *prefered* m-sequences according to the study performed in [23] is very similar to those of Gold sequences, we omit them from the comparison in this paper.

The rest of the paper is organized as follows. Section II introduces the basic fundamentals and trade-offs of PMCW radar design, as well as the importance of the ambiguity function in phase-coded waveform design. Section III gives a detailed investigation of the three most promising binary sequences and their performance comparison. In Section IV, the transmission schemes that can be used in an automotive radar are explained. For proposed MIMO transmission schemes, Section V discusses the auto- and cross-correlation performance of the received signal under a Doppler-shift. Finally, conclusions are drawn in Section VI.

II. Preliminaries

This section summarizes some required fundamentals for a clear understanding on MIMO phase-modulated waveforms. In a PMCW radar, the waveforms are coded using sequences from a certain set, or codebook, referred to as $\mathcal{S}$. Here, $|\mathcal{S}|$ denotes the sequence set size. Each codeword, or sequence in $\mathcal{S}$ is constructed out of symbols from alphabet such that the sequence is of length L_c. Binary Phase-Shift Keying (BPSK) can be used to modulate the codes from a predefined alphabet according to the phases $\phi(t) \in \{0, \pi\}$ on a single-carrier frequency f_c, resulting in the transmitted radio-frequency (RF) signal

$$s_{RF}(t) = e^{j2\pi f_c t + j\phi(t)} \tag{1}$$

All codes derived from a code family exhibit similar properties in terms of periodic autocorrelation function (PACF) and periodic cross-correlation function (PCCF). The codes determine the radar's performance in terms of dynamic range and transmit (TX) orthogonality, whose can independently be characterized by theoretical metrics as the periodic autocorrelation function (PACF) and periodic cross-correlation function (PCCF), denoted by R_{xx} and R_{xy} respectively

$$R_{xx}[k] = \sum_{n=0}^{L_c-1} c_x[n] c_x^*[n-k], \tag{2}$$

$$R_{xy}[k] = \sum_{n=0}^{L_c-1} c_x[n] c_y^*[n-k], \tag{3}$$

where c_x and c_y are periodic sequences and, hence, are taken modulo L_c, and s^* denotes the complex conjugate. A single-period of c_x can be used to determine the correlation outputs.

Ideally, to avoid the effect of target masking and cross-influencing of concurrently transmitted waveforms, the PACF and PCCF should hold

$$R_{xx}[k] \neq 0 \quad \text{for mod}(k, L_c) = 0, \tag{4}$$

$$R_{xx}[k] = 0 \quad \text{for mod}(k, L_c) \neq 0, \tag{5}$$

$$R_{xy}[k] = 0 \quad \text{for all } k. \tag{6}$$

However, there are no perfect binary sequences possessing these characteristics. Sarwate [24], Welch [25] and Tang-Fan [26] have defined different lower bounds for different kind of sequences. Let us denote, ψ_a as the maximum sidelobe level of the PACF, whereas ψ_c is used to refer to the maximum value of the PCCF. Here with $\psi_m = \max\{\psi_a, \psi_c\}$, the famous Welch Bound presents a lower bound for binary sequence [25]

$$\psi_m^2 \geq \frac{(|\mathcal{S}| - 1)L_c^2}{|\mathcal{S}|L_c - 1}. \tag{7}$$

Furthermore, in practice, the coded waveforms are acquired together with possible other transmitters' waveforms in free space, being sampled by the analog-to-digital converter (ADC) after the low noise amplifier (LNA) and down-converter stage, affected by independent noise samples.

A. Trade-Offs in PMCW

The theoretical limitation, shown by the inequality of (7), implies that in high-demanding designs trade-offs need to be made among imperfections in correlations values, sequence set size, or the code length. Here, the sequence set size relates to the number of (semi-)orthogonal channel accesses, while the code length influences the maximum unambiguous distance and velocity of a target observed by a radar. The maximum unambiguous distance R_u and maximum unambiguous velocity v_u are defined by, respectively

$$R_u < \frac{c\, T_c L_c}{2}, \tag{8}$$

$$|v_u| < \frac{\lambda}{4 T_c L_c}. \tag{9}$$

where c is speed of light, T_c is the duration of a chip, and λ is the wavelength. Eq. (8) and (9) induce a lower and upper bound

on the code length, L_c as follows

$$\frac{2R_u}{cT_c} < L_c < \frac{\lambda}{4\, v_u T_c}. \tag{10}$$

B. Ambiguity Function

Non-zero relative radial velocities between the source and a possible target causes the waveform to distort. While moving targets cause the wideband waveforms to contract and expand (in time-domain), narrowband waveforms experience a frequency shift of their carrier frequency by the so-called Doppler frequency f_D. The narrowband assumption holds in automotive applications for the predefined specifications of the so-called Short Range Radar (SRR), Medium Range Radar (MRR), and Long Range Radar (LRR) as given in [27]. The conditions for which this narrowband assumption can be taken into account are,

$$\frac{B}{f_c} < 0.1, \tag{11}$$

$$vT_f << \frac{c}{2B}, \tag{12}$$

where B denotes the receiver bandwidth, f_c is the carrier frequency, v is the target's velocity, and $T_f = ML_cT_c$ is the measurement time of a single frame. After neglecting the high order terms, the Doppler shift is usually be approximated by $f_D = 2v/\lambda$. Thus, we can write the received signal, that is input to the LNA, under the narrowband assumption [2] as

$$\begin{aligned} r(t) &= s_{RF}(t-\tau) \\ &= e^{j2\pi f_c t + j\phi(t-\tau)} \underbrace{e^{-j2\pi f_D t}}_{\text{Doppler shift}} \underbrace{e^{j4\pi f_c \frac{R_0}{c}}}_{\text{range phase offset}} \end{aligned} \tag{13}$$

where $\tau = 2(R_0 + vt)/c$ denotes the round-trip time-delay. In radar, the assumed frequency deviations, as well as time delays, can severely impact the matched filter's performance. In this paper, we use the narrowband ambiguity function to observe the matched filter performance of each code family, which is determined by

$$\chi(\tau, f_D) = \int_{-\infty}^{\infty} s(t)s^*(t-\tau)e^{-j2\pi f_D t}dt. \tag{14}$$

III. Binary Code Families

This paper considers three encouraging binary code families: the Gold sequence (closely related to Kasami), APAS sequence, and Zero Correlation Zone (ZCZ) sequences.

A. Gold Sequence

Gold codes are nowadays implemented in telecommunications (CDMA) and satellite communications (GPS). This type of application takes advantage of the fact that large sets of sequences can be generated with relatively good cross-correlation properties [28]. Also, the sets can be easily constructed using only two *prefered* m-sequences. The Gold sequence is of length $L_c = 2^n - 1$ and is generated from two *prefered* m-sequences that are circularly shifted and modulo-2 added. However, the number of shift registers n must satisfy $mod(n, 2) = 1$ or $mod(n, 4) = 2$ [28]. The resulting Gold code set of period L_c, of a selected *prefered* m-sequence pair **a** and **b**, can mathematically be represented as

$$S_G(\mathbf{a}, \mathbf{b}) = \left\{\mathbf{a} \otimes D^l\mathbf{b}\right\} \quad \text{with} \quad l = 0, 1, \ \ldots \ L_c - 1. \tag{15}$$

The operator D represents a shift to the periodic sequence by l positions to the right. Then, the set size contains $\mathbf{a}$, $\mathbf{b}$ and $(2^n - 2)$ shifted versions of $\mathbf{b}$, therefore, resulting in a sequence set size is equal of $|\mathcal{S}_G| = 2^n + 1$.

B. Almost Perfect Autocorrelation Sequence (APAS)

In 1992, Wolfmann was first to generate a binary sequence whose autocorrelation properties were perfect autocorrelation function except for one lag, known as the Almost Perfect Autocorrelation Sequences (APAS) [29]. He created the sequences up to the size of 100 based on an exhaustive search, which can be found in the appendix of [29]. In [30], Pot and Bradley demonstrate an algorithm that can generate APAS sequences of longer lengths, which is based on *p*-ary [31] m-sequences. The sequence of interest was deeply analyzed by Van Thillo *et al.*, whereas the following properties have been concluded of the L_c-sized APAS sequences [32]:

1) Periodic autocorrelation function has an L_c-amplitude peak for the in-phase value. The out-of-phase values are zero for all non-zero shifts are zero, except for two lags, at $\pm L_c/2$, where two negative peaks are found.
2) The zero-autocorrelation zone is therefore $L_c/2 - 1$.
3) The amplitude of the negative peaks is measured to be $-L_c + 4$.
4) The sequence length must be a multiple of 4. Also, $L_c/2 - 1$ must be a prime power e.g. of the form $L_c/2 - 1 = p^r$ with p prime and r a positive integer.
5) The sequence set size is given by
$$|\mathcal{S}_A| = \begin{cases} \frac{\phi(N/4)}{2r}, & \text{if } \mod(N/2 - 1,\ 4) = 1 \\ \frac{\phi(N/4)}{r}, & \text{if } \mod(N/2 - 1,\ 4) = 3 \end{cases}$$
where $\phi(n)$ refers to Euler's totient function [33].

C. Zero Correlation Zone (ZCZ) Sequence

ZCZ sequences are binary sequences with special correlation properties. For both the PACF and PCCF, the ZCZ sequences are designed such that the PACF/PCCF have zero correlation values in a specified zone (Z_{CZ}). Generally, a ZCZ sequence is defined using a triplet notation (L_c, $|\mathcal{S}_Z|$, Z_{CZ}), where L_c refers to the code length, $\mathcal{S}_Z$ notes the sequence set size, and Z_{CZ} defines the width of the zero-correlation zone.

$$\begin{aligned} Z_{CZ} = \max\{Z_{CZ} : R_{x,y}[k] = 0,& \\ &\text{where } (|k| \le Z_{CZ} \text{ and } x \ne y) \\ &\text{or } (0 < |k| \le Z_{CZ} \text{ and } x = y)\}. \end{aligned} \tag{16}$$

The last decades several algorithms have been developed for construction of *optimal* ZCZ sequence set. The random variables in these algorithms are again L_c, $|\mathcal{S}_Z|$ and Z_{CZ}. Binary ZCZ sequences have been proven by Tang-Fan [26] to be upper

TABLE I
CHARACTERISTICS OF THREE ALGORITHMS FOR GENERATING ZCZ SEQUENCES

Algorithm	Triplet $(L_c, \mathcal{S}_Z, Z_{CZ})$
[34]	$(2^{2n}L_0, 2^{n+1}, 2^n + 1)$
[35]	$(2^{2n+1}, 2^{n+1}, 2^{n-1}L_0 + 1)$
[36]	$(2^{p+2} \cdot n, 2n, 2^p)$

bounded by,

$$|\mathcal{S}_Z|(Z_{CZ} + 1) \leq L_c, \tag{17}$$

where equality implies optimality. Table I lists three different algorithms from [34]–[36] having a different triplet, which have been implemented. We found that the algorithm from [36] can provide the most flexible triplet; w.r.t the code length, zero-correlation zone and the number of possible channel accesses. Therefore, in this paper the ZCZ sequences are generated using this algorithm.

D. Performance Comparison of Gold, APAS, and ZCZ

1) Periodic Autocorrelation Function: The PACF is a measure that translates how a reflector's response in the range profile will look like. From Eq. (4)–(5), we see the command for a single peak at the round-trip delay and zero sidelobes. In Appendix A, Fig. 7 represents the PACF and PCCF of the Gold, APAS and ZCZ sequences, respectively. The results show that the Gold codes exhibit deterministic non-zero autocorrelation values, while the APAS and ZCZ have a specified width of out-of-phase lags where the autocorrelation values are zero. These widths are $L_c/2 - 1$ and Z_{cz}, respectively, which can be strategically considered in the design process of the radar.

2) Periodic Cross-Correlation Function: In case two or more transmit antennas are radiating unique coded waveforms simultaneously, the impact of inter-element interference is analyzed by the PCCF. Referring to fully orthogonal waveforms, and therefore no inter-element interference, Eq. (6) must be satisfied for all combinations of the concurrently transmitted codewords. Likewise to its PACF, the Gold code shows similar deterministic correlation values for all lags. The cross-correlation values of the APAS sequence are not deterministically known, but show to be relatively high as we observe in Fig. 7. The ZCZ sequences bypass the aforementioned Welch bound from Eq. (7), within the interference-free window of Z_{cz} lags.

3) Ambiguity Function: The analysis in Section III-D1 and Section III-D2 shows the theoretical correlation functions, where the PACF is a cut of the ambiguity function along the 0 Hz Doppler axis. As mentioned earlier, Doppler distortions can influence the performance the code's correlation characteristics. The Doppler shift might effect the matched filter performance, which is shown using the periodic ambiguity function in Fig. 1. For the three specific code families, we list the following findings on the ambiguity functions:

i) The non-delayed and non-Doppler shifted waveform shows a peak and reappears after each period $|\chi(nT_r, 0)|$, with $n = 0, 1, \ldots, M - 1$.
ii) The zero-Doppler cut of the ambiguity function, $|\chi(\tau, 0)|$, exposes the same output as found in Section III-D1.

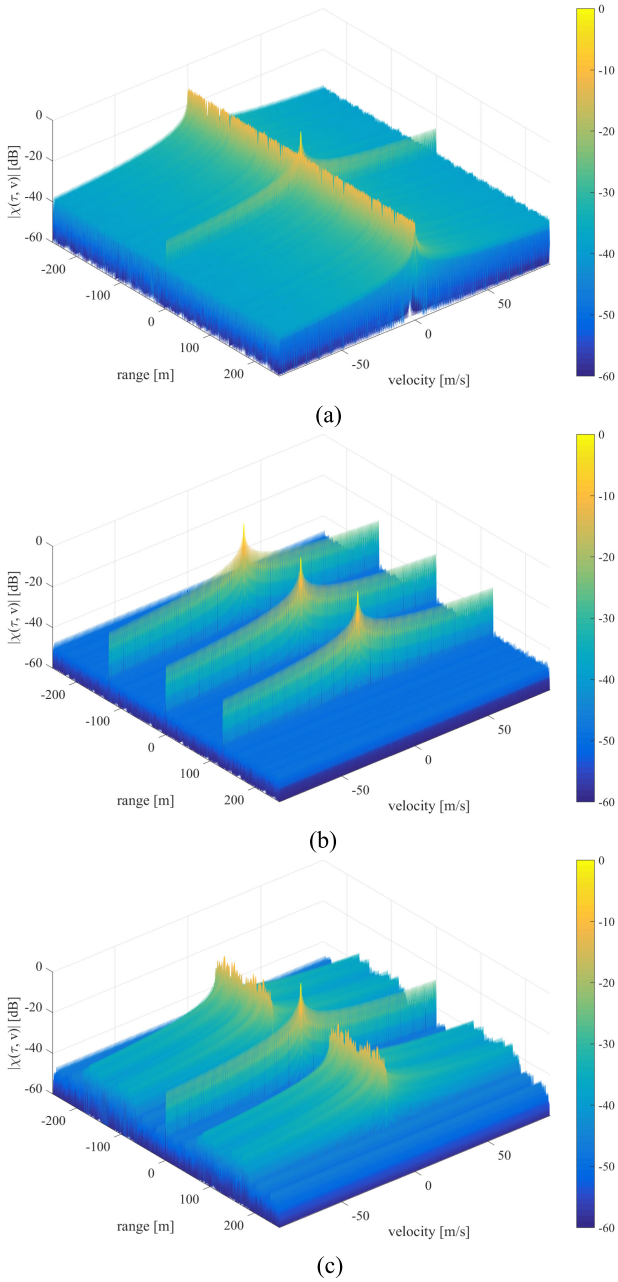

Fig. 1. Ambiguity Function of different code families having a frame time of $T_f = 5$ ms and a bit rate of $R_c = 1/T_c = 300$ MHz. (a) Gold code (1023), (b) APAS code (1020), and (c) ZCZ code (1024).

iii) For a non-zero Doppler shift the matched filter's output is a factor smaller than the zero-Doppler cut. The decline is according to the sinc-pattern, e.g. the first side lobe in Doppler is -13.48 dB lower compared to the main lobe.

IV. PMCW MIMO TX SCHEMES

Generally, in continuous wave radar the periods are repeated to a predefined dwell time to suffice the velocity resolution. In PMCW, the codes are repeated K_T times with a duty cycle of 100% to retain the periodic correlation characteristics. However, the MIMO transmission is part of the design space and can be

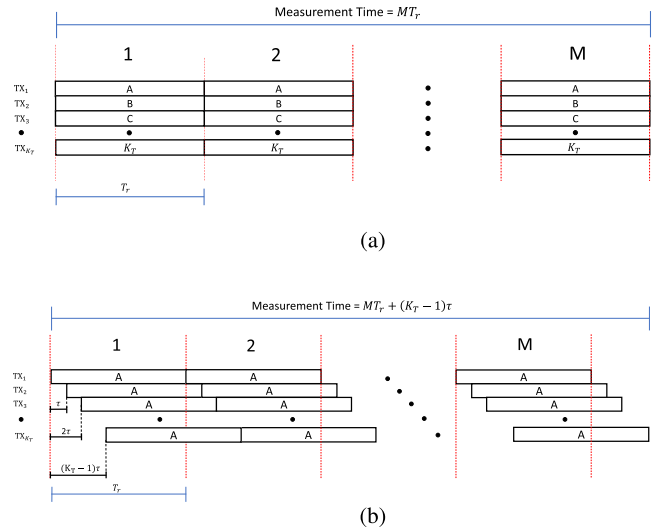

Fig. 2. Different MIMO Transmit schemes for phases coded automotive radar. (a) Code division multiplexing (CDM), and (b) Time-division multiplexing (TDM).

used to utilize the enhanced code properties while transmitting with K_T antennas. In this section, we explain our design strategies that strive for maximum performance by enhancing the best correlation characteristics of each code family.

A. Code Division Multiplexing

The trivial transmission scheme, that has also been used in CDMA systems, is code division multiplexing with a simultaneous starting time, t_0, for all the transmitting elements. In this scheme, as shown in Fig. 2(a) , each antenna radiates a unique code

$$\begin{aligned} s_1(t) &= \sum_{m=0}^{M-1}\sum_{l=0}^{L_c-1} c_1(t)\ \text{rect}\left(\frac{t-lT_c-mT_r}{T_c}\right) \\ s_2(t) &= \sum_{m=0}^{M-1}\sum_{l=0}^{L_c-1} c_2(t)\ \text{rect}\left(\frac{t-lT_c-mT_r}{T_c}\right) \\ &\vdots \\ s_{K_T}(t) &= \sum_{m=0}^{M-1}\sum_{l=0}^{L_c-1} c_{K_T}(t)\ \text{rect}\left(\frac{t-lT_c-mT_r}{T_c}\right). \end{aligned} \tag{18}$$

As $s_1(t), \ldots, s_N(t)$ are simultaneously transmitted and received, the cross-correlation properties of the transmitted codes $c_1(t), \ldots, c_N(t)$ deeply determine the severeness of coexistence. This MIMO transmission technique has been used for the Gold and ZCZ Sequence.

B. Time Division Multiplexing

In [10], a different MIMO transmission scheme was proposed where a single sequence was transmitted by K_T transmit elements in a time-staggered fashion (see Fig. 2(b)). Although other techniques like outer-coding also exist [10], we have restricted ourselves to the time-staggered TDM. It was specifically designed for sequences having excellent autocorrelation properties, like APAS, and hence worse cross-correlation properties. Each antenna in the array starts transmitting at a different time instant, resulting in the time-staggered profile that could be written as

$$\begin{aligned} s_1(t) &= \sum_{m=0}^{M-1}\sum_{l=0}^{L_c-1} c_1(t)\ \text{rect}\left(\frac{t-lT_c-mT_r}{T_c}\right) \\ s_2(t) &= \sum_{m=0}^{M-1}\sum_{l=0}^{L_c-1} c_1(t-\tau_A)\ \text{rect}\left(\frac{t-\tau_A-lT_c-mT_r}{T_c}\right) \\ &\vdots \\ s_{K_T}(t) &= \sum_{m=0}^{M-1}\sum_{l=0}^{L_c-1} c_1\left(t-(K_T-1)\tau_A\right) \\ &\quad \text{rect}\left(\frac{t-(K_T-1)\tau_A-lT_c-mT_r}{T_c}\right). \end{aligned} \tag{19}$$

where τ_A is the artificially induced inter-element delay. The autocorrelation function contains $L_c/2-1$ zero-output values, which leads to a minimum delay of

$$\tau_A \geq \frac{L_c\, T_c}{2K_T}, \tag{20}$$

showing the dependency on the number of transmit elements. Here, τ_A is configured such that it exceeds the round-trip time corresponding to the required maximum distance.

V. Doppler Tolerance

Waveform orthogonality has been analyzed by performing simulations in the MATLAB environment with the radar parameters shown in Table II. In this study, a model of the PMCW transceiver is used that does not include any non-linear effects, and, therefore, has a comparable front-end setup and digital signal processing flow as presented in [10, Fig. 1]. For simplicity, we have chosen for a Multiple Input Single Output (MISO) setup, as the number of receive array elements does not influence the Doppler distortions of the waveform. The simulated radar contains 16 transmit elements, hence this section entails the orthogonality effects for 16 channel accesses. From Table II, the reader can derive that the processing gain for each of the three code family setups has been equalized, while having similar a receiver noise bandwidth, which enables us to compare noise power levels, as well as the powers of eventual artifacts.

A. In Range-Doppler Map

Fig. 3 shows the Range-Doppler (range-velocity) output for a single static target at $R_0 = 20$ m, while the other case presents the output for a moving target with 40 m/s. In fact, the two main consequences of the Doppler effect, which are caused due to imperfections in the autocorrelation and non-orthogonality, are:

1) Decrease in Target Peak Power: All inspected code families show a similar effect with respect to a target's peak power when it is affected by Doppler. The degradation in peak power for increasing relative velocities impairs exponentially

TABLE II
MRR MIMO SYSTEM PARAMETERS

Parameter	Symbol	Values					
		Gold		**ZCZ**		**APAS**	
Number of transmit antennas	K_{T}	16		16		16	
Number of receive antennas	K_{R}	1		1		1	
MIMO Multiplexing scheme		CDM		CDM		TDM	
Code length	L_c	2047		4096		5184	
Chip duration	T_{c}	3.33	ns	3.33	ns	3.33	ns
Duration of period	T_{r}	6.82	µs	13.65	µs	17.28	µs
Number of periods	M	1465		732		578	
Number of FFT points in Doppler processing	N_{FFT}	2048		1024		1024	
Total duration of a single transmit frame	T_{f}	9.996	ms	9.99	ms	10.00	ms
Range resolution	ΔR	0.5	m	0.5	m	0.5	m
Maximum distance	R_u	1022.8	m	2046.6	m	81.0	m
Maximum zero-correlation distance	R_{cz}	-		64	m	81.0	m
Velocity resolution	Δv	0.19	m/s	0.19	m/s	0.19	m/s
Maximum velocity	v_u	139.0	m/s	69.49	m/s	55.15	m/s

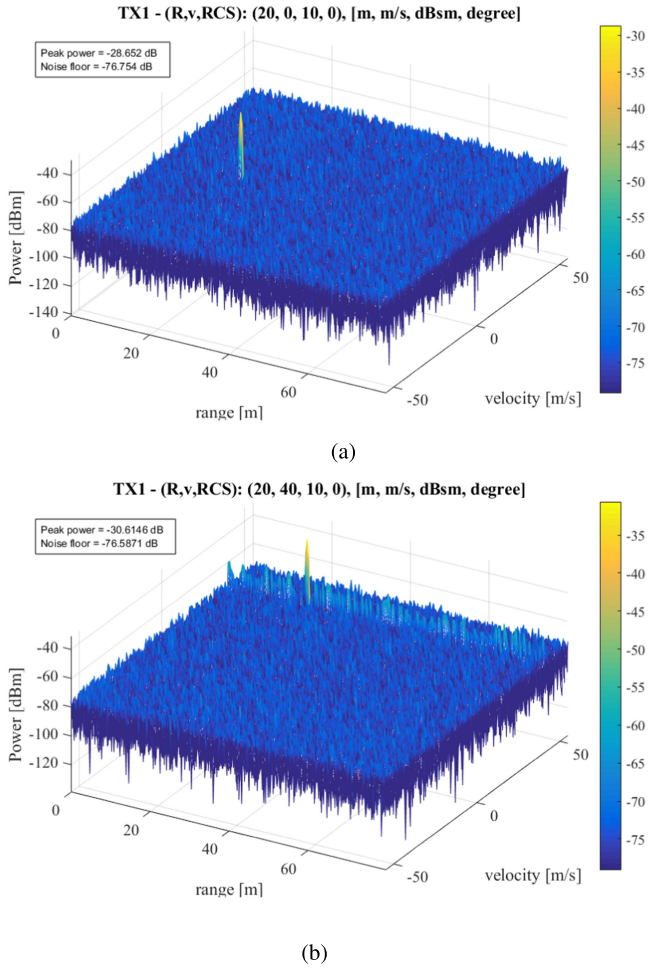

Fig. 3. Range-Doppler map of different code families for suitable automotive radar applications. (a) APAS (5184) with a static target, and (b) APAS (5184) with a moving target (40 m/s).

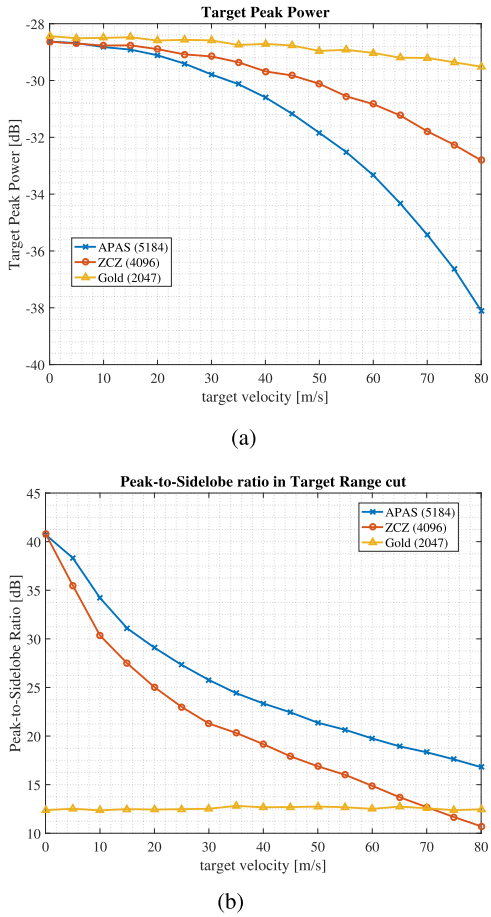

Fig. 4. Doppler tolerance for target's range cut. (a) Doppler tolerance of the target peak power, and (b) Doppler tolerance of peak-to-sidelobe ratio (PSLR).

as L_c increases (see Fig. 4(a)), showing the Doppler intolerance of BPSK phase-coded waveforms. The absolute peak power determines the ability to detect targets from noise/interference. Regarding the Signal-to-Noise (SNR) reduction caused by Doppler distortions, the Gold sequence with $L_c = 2047$ is least effected. In this case, the peak power degrades with a maximum of 1 dB up to 80 m/s.

2) Increase in Range Sidelobes: Secondly, the Doppler reflections causes artifacts within the target's range cut. The ideal properties of the autocorrelation function of the APAS sequence are lost. In Fig. 4(b), one can observe that the TDM configuration of the APAS sequence performs best in peak-to-(range)-sidelobe ratio. While its target peak degrades the fastest, its peak-to-sidelobe ratio performs relatively well, meaning that its sidelobes do not come up as fast compared to the other configurations. The autocorrelation properties of the

APAS hence perform better in the presence of Doppler than the auto- and cross-correlations of the ZCZ sequence. The Gold sequence retains near-similar range sidelobe levels as mainly its theoretically-defined inherent range sidelobes are rather high.

B. In Range-Angular Map

The reception of angular information from phase-modulated waveforms is discussed in this section. The assumption of the virtual Uniform Linear Array (ULA) has been taken into consideration. Let us assume that omnidirectional transmitters are deployed. Therefore, the received signal from L targets can be defined as

$$\mathbf{s}_R(t) = \sum_{l=1}^{L} \beta_l \, \mathbf{a}_R(\theta_l) \, \mathbf{a}_T^T(\theta_l) \, \mathbf{s}_{RF}(t - \tau_l). \tag{21}$$

with $\mathbf{s}_{RF}(t)$ being the $N \times 1$ transmit modulated symbol vector, and $\mathbf{a}_R(\theta)$ and $\mathbf{a}_T(\theta)$ being the transmit and receive steering vector, respectively given by:

$$\mathbf{a}_T(\theta) = \left[1, \; e^{j2\pi d_T \frac{\sin(\theta)}{\lambda}}, \quad \ldots, \; e^{j2\pi d_T (K_T - 1) \frac{\sin(\theta)}{\lambda}}\right]^T, \tag{22}$$

$$\mathbf{a}_R(\theta) = \left[1, \; e^{j2\pi d_R \frac{\sin(\theta)}{\lambda}}, \quad \ldots, \; e^{j2\pi d_R (K_R - 1) \frac{\sin(\theta)}{\lambda}}\right]^T. \tag{23}$$

with d_T and d_R being the inter-element distance between the transmit antennas and the receive antennas, and K_T and K_R being the number of transmit and receive antenna elements. In coherent MIMO radar, it is possible to retrieve angular information of the reflected signals by stacking the measurement data of the receive antennas, and creating a *virtual* antenna array. In the case of orthogonal channels, we can write the $\mathbf{a}_R(\theta)\mathbf{a}_T^T(\theta)$ product as a diagonal matrix, which we can vectorize. Therefore, this product can be rewritten as the Kronecker product of both vectors

$$\mathbf{a}_V(\theta) = \mathbf{a}_T(\theta) \otimes \mathbf{a}_R(\theta). \tag{24}$$

Using prior knowledge from the array dimensions from (24), we are able to retrieve the incident angle of the reflected waveforms by performing a spectral analysis [37]. Eventually, the angular spectrum is presented in Fig. 6 for static targets, as well as moving targets.

Below, we give a comparison on the performance of the phase-coded waveforms in the angular domain.

First of all, we address the (FFT) processing gain that can be achieved by taking a FFT over the spatial samples in order to retrieve angular information from the phase rotations of the virtual array geometry. The maximum achievable processing gain can then be denoted as

$$G_{P,ang} = 10 \log_{10}(K_v) + L_{win} = 9.63 \text{ dB}, \tag{25}$$

where $K_v = K_T = 16$ denotes the number of virtual antenna elements, and

$$L_{win} = \frac{1}{N} \frac{\left\| \sum_{n=0}^{N-1} w[n] \right\|^2}{\sum_{n=0}^{N-1} \|w[n]\|^2} \tag{26}$$

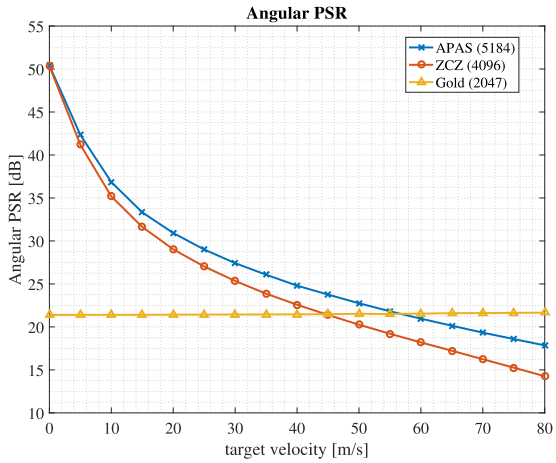

(a)

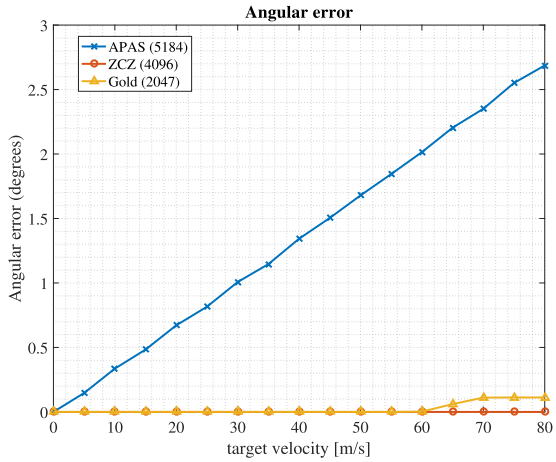

(b)

Fig. 5. Doppler Tolerance in Range-Angular Map; w.r.t (a) Angular Peak-to-Sidelobe ratio, and (b) Estimated angular error.

accounts for the coherent processing loss induced by the windowing. For example, the Chebyshev window causes an -2.40 dB SNR loss for $K_v = 16$. By this windowing, the sidelobe level of -80 dB is achieved.

The effects of Doppler in the range-azimuth plane can be explained by following metrics.

1) Increase in Range Sidelobes: Analogous to the range-Doppler domain, Doppler-affected binary phase-coded waveforms show decreased peak-to-sidelobe levels in the range-Angular domain for increasing target velocity (see Fig. 5(a)). Basically, the nonidealities in the angular domain is a direct consequence of the range sidelobes which arose in the range-Doppler domain. The Doppler effects disrupt the orthogonality condition for the virtual array, as the $\mathbf{a}_R(\theta)\mathbf{a}_T^T(\theta)$ product contains non-diagonal terms and cannot be defined as the Kronecker product of (24). Therefore, the Doppler induced non-orthogonal waveforms for the APAS and ZCZ family show artifacts in Fig. 6(b)–6(c), showing a specific family sensitivity pattern. The Gold sequence is inherently non-orthogonal, hence the Gold code's angular spectrum, shown in Fig. 6(a), is imperfect and shows a noise-like behaviour.

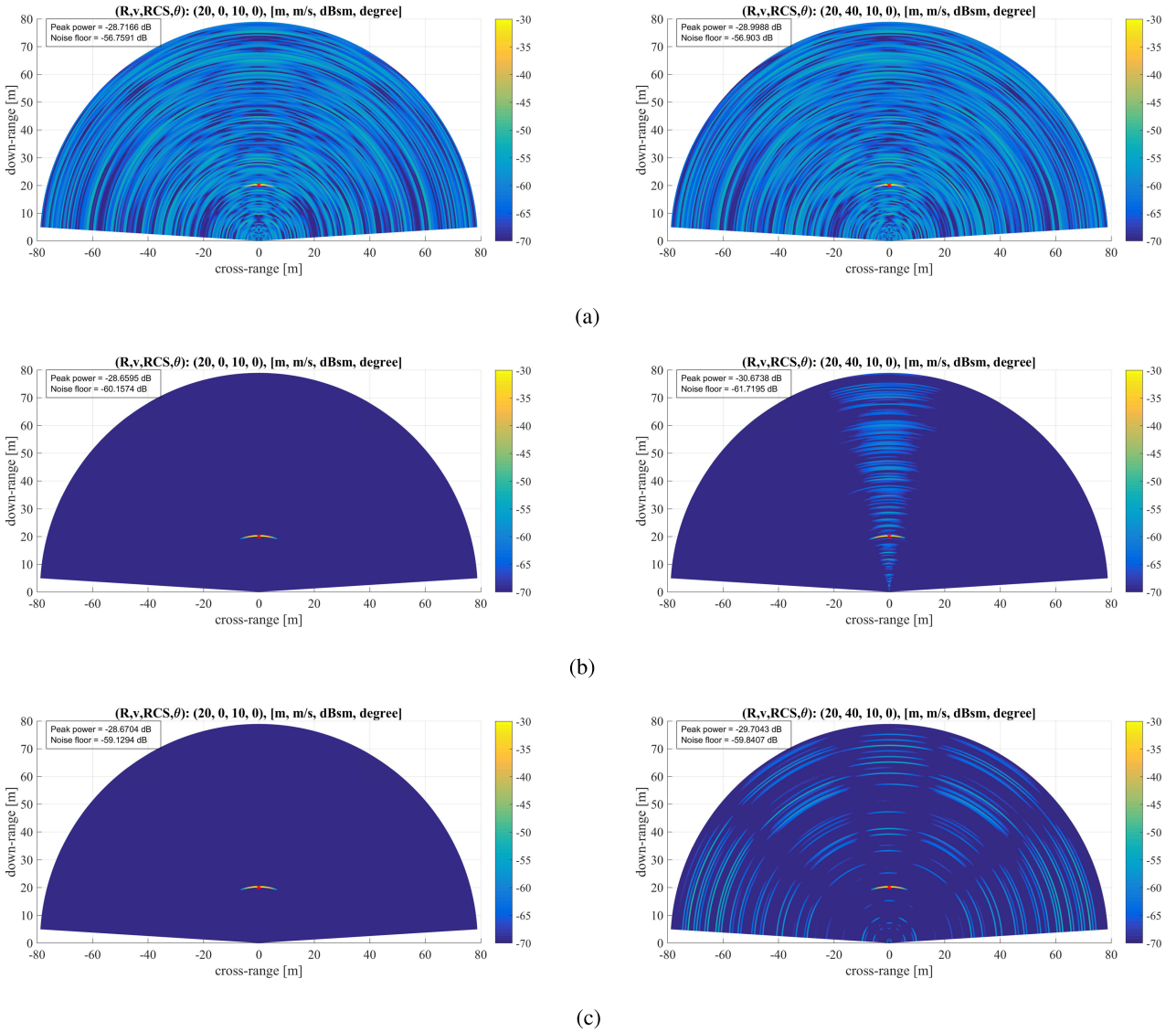

Fig. 6. Range-Angular Map: Sensitivity comparison for the (a) Gold (2047), (b) APAS (5184), and (c) ZCZ (4096). The left figures show the angular spectrum output for a static target, while the rightmost figures show the angular spectrum output for a moving target with 40 m/s.

2) Error in Angular Estimation: For the APAS sequence, the artifacts are directed only in the beam that corresponds to the width of the main lobe. In this case, the energy of the artifact is higher compared to the case for the ZCZ sequence and is also present before the target's location. Besides, in contrast to the Gold and ZCZ sequences that are transmitted concurrently using CDM, the APAS sequence incorrectly estimates the target's angular position in the presence of Doppler. The error is linearly dependent on the target's velocity, as illustrated in Fig. 5(b). This phenomenon is because a nonconcurrent transmission scheme is applied, which does not take account for the position changes during the sequential TX activations for moving targets. The received signal at antenna 1 is a summed version of time-staggered transmitted waveforms

$$s_{rx,1}(t) = \sum_{n=1}^{N_T} s_{RF}(t - \tau_{A,n} - t_{d,n})\, e^{j2\pi(n-1)d_t \sin(\theta)/\lambda} \quad (27)$$

with n denoting the n^{th} of the transmit array, $\tau_{A,n}$ the time-staggered induced delay and $t_{d,n}$ the round-trip delay. For moving targets, unfortunately $t_{d,n}$ changes over time as targets are non-stationary. To solve this issue, displacement compensation for moving targets can be implemented. A similar technique can then be applied as proposed in [38] that compensates for motion in TDMA FMCW MIMO radar systems.

VI. Conclusion

In this paper, we have investigated the orthogonality characteristics and such performance indicators as side-lobe levels of target images in Range-Doppler and Range-Azimuth planes of phase-modulated waveforms for automotive radar applications. Particularly, the three most-promising binary code families (Gold, APAS, and ZCZ sequences) have been compared in their performance for short to medium range automotive radar setups. Novel insights on how the radar performance is effected for

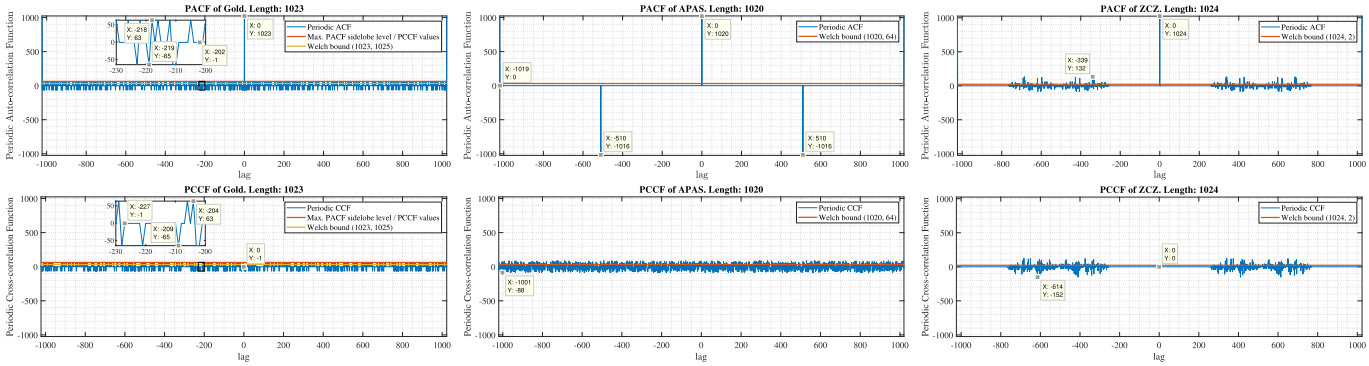

Fig. 7. PACF (top) and PCCF (bottom) of Gold(1023), APAS(1020), and ZCZ(1024), respectively.

the selected MIMO transmit schemes have been gained, while including the inherent code properties.

This paper starts with a theoretical analysis on the code family's inherent correlation properties, including the ambiguity function. Then, we show that target velocity degrades the code inherent correlation performance (decreases peak power and rises side lobes). This degradation becomes more severe with code length increase. Secondly, each code family is found to be sensitive to Doppler in a different way, depending how the bits in the codes are structured. The sensitivity due to Doppler can be stated as: the Gold sequences seem to be negligibly effected, while the APAS and ZCZ sequences show significant degradations with respect to losses in peak power and increasing range sidelobes, thus causing SNR reduction. On the other side, in case of the APAS sequence, the target's velocity bin contains less apparent range sidelobes as the peak-to-sidelobe ratio outperforms those of the Gold and ZCZ sequence. Therefore, we can claim that the time-staggered transmit scheme with autocorrelation properties only (while introducing azimuthal errors) results in improved performance compared to code division multiplexing with auto- and cross-correlation properties.

The overall conclusion is that the Doppler shifts reduces the detection performance to a certain extent for phase-coded radar systems in both the Range-Doppler and Range-Angular maps. Still, the resilience to the interference and the hardware imperfections should also be studied to identify the best available phase code for automotive radar applications.

APPENDIX A
PERIODIC AUTO- AND CROSS-CORRELATION FUNCTIONS

Fig. 7 presents the PACF and PCCF of the Gold sequence, APAS, and ZCZ sequences.

ACKNOWLEDGMENT

The authors would like to thank NXP Semiconductors for providing auspicious facilities to the first author, as most of his results were obtained in their office in Eindhoven.

REFERENCES

[1] S. M. Patole, M. Torlak, D. Wang, and M. Ali, "Automotive radars: A review of signal processing techniques," *IEEE Signal Process. Mag.*, vol. 34, no. 2, pp. 22–35, Mar. 2017.
[2] A. van der Veen and G. Leus, *Signal Processing for Communications*, vol. 6, 2005.
[3] X. Zhuge and A. G. Yarovoy, "Sparse multiple-input multiple-output arrays for high-resolution near-field ultra-wideband imaging," *IET Microw., Antennas Propag.*, vol. 5, no. 13, pp. 1552–1562, Oct. 2011.
[4] R. Feng, F. Uysal, P. Aubry, and A. Yarovoy, "MIMO-Monopulse target localization for automotive radar," *IET Radar, Sonar Navigation*, vol. 12, no. 10, pp. 1131–1136, Oct. 2018.
[5] L. Guosui, G. Hong, and S. Weimin, "Development of random signal radars," *IEEE Trans. Aerosp. Electron. Syst.*, vol. 35, no. 3, pp. 770–777, Jul. 1999.
[6] R. Norland, "Digital signal processing in binary phase coded CW multistatic radar," in *Proc. Int. Conf. Radar*, Sep. 2003, pp. 299–302.
[7] R. M. Davis, R. L. Fante, and R. P. Perry, "Phase-coded waveforms for radar," *IEEE Trans. Aerosp. Electron. Syst.*, vol. 43, no. 1, pp. 401–408, Jan. 2007.
[8] J. D. Zhang, X. H. Zhu, and H. Q. Wang, "Adaptive radar phase-coded waveform design," *Electron. Lett.*, vol. 45, no. 20, pp. 1052–1053, Sep. 2009.
[9] F. Uysal, "Phase-coded FMCW automotive radar: System design and interference mitigation," *IEEE Trans. Veh. Technol.*, 2019.
[10] A. Bourdoux, U. Ahmad, D. Guermandi, S. Brebels, A. Dewilde, and W. V. Thillo, "PMCW waveform and MIMO technique for a 79 GHz CMOS automotive radar," in *Proc. IEEE Radar Conf.*, May 2016, pp. 1–5.
[11] H. Haderer, R. Feger, and A. Stelzer, "A comparison of phase-coded CW radar modulation schemes for integrated radar sensors," in *Proc. 44th Eur. Microw. Conf.*, Oct. 2014, pp. 1896–1899.
[12] T. J. Riedl and A. C. Singer, "Broadband doppler compensation: Principles and new results," in *Proc. Conf. Rec. 45th Asilomar Conf. Signals, Syst. Comput.*, Nov. 2011, pp. 944–946.
[13] Z. Matousek, J. Ochodnicky, M. Babjak, and J. Puttera, "Doppler compensation for binary phase-coded radar signals in presence of noise jamming," in *Proc. 17th Int. Radar Symp.*, May 2016.
[14] A. M. D. Turkmani and U. S. Goni, "Performance evaluation of maximal-length, gold and kasami codes as spreading sequences in CDMA systems," in *Proc. 2nd IEEE Int. Conf. Universal Pers. Commun.*, Oct. 1993, vol. 2, pp. 970–974.
[15] M. Golay, "Complementary series," *IRE Trans. Inf. Theory*, vol. 7, no. 2, pp. 82–87, Apr. 1961.
[16] K. R. Griep, J. A. Ritcey, and J. J. Burlingame, "Poly-phase codes and optimal filters for multiple user ranging," *IEEE Trans. Aerosp. Electron. Syst.*, vol. 31, no. 2, pp. 752–767, Apr. 1995.
[17] R. Frank, "Polyphase complementary codes," *IEEE Trans. Inf. Theory*, vol. 26, no. 6, pp. 641–647, Nov. 1980.
[18] M. Jankiraman, N. Willis, and H. Griffiths, *Design of Multi-Frequency CW Radars* (Electromagnetics and Radar). London, U.K.: Institution of Engineering and Technology, 2007. [Online]. Available: https://books.google.nl/books?id=r0VIkCoihr8C

[19] S. W. Golomb, "Two-valued Sequences with Perfect Periodic Autocorrelation," *IEEE Trans. Aerosp. Electron. Syst.*, vol. 28, no. 2, pp. 383–386, Apr. 1992.

[20] N. Levanon and E. Mozeson, *Radar Signals*. Hoboken, NJ, USA: Wiley, 2004.

[21] A. Pezeshki, A. R. Calderbank, W. Moran, and S. D. Howard, "Doppler resilient golay complementary waveforms," *IEEE Trans. Inf. Theory*, vol. 54, no. 9, pp. 4254–4266, Sep. 2008.

[22] J. Eaves and E. Reedy, *Principles of Modern Radar*. New York, NY, USA: Nostrand, 1987. [Online]. Available: https://books.google.nl/books?id=xaZTAAAAMAAJ

[23] J. Overdevest, "Interference in 79 GHz Phase-Coded Automotive Radar," Master's thesis, Delft University of Technology, Delft, The Netherlands, 2018.

[24] D. Y. Peng and P. Z. Fan, "Generalised sarwate bounds on periodic autocorrelations and cross-correlations of binary sequences," *Electron. Lett.*, vol. 38, no. 24, pp. 1521–1523, Nov. 2002.

[25] L. Welch, "Lower bounds on the maximum cross correlation of signals (Corresp.)," *IEEE Trans. Inf. Theory*, vol. 20, no. 3, pp. 397–399, May 1974.

[26] X. H. Tang, P. Z. Fan, and S. Matsufuji, "Lower bounds on correlation of spreading sequence set with low or zero correlation zone," *Electron. Lett.*, vol. 36, no. 6, pp. 551–552, Mar. 2000.

[27] J. Hasch, E. Topak, R. Schnabel, T. Zwick, R. Weigel, and C. Waldschmidt, "Millimeter-wave technology for automotive radar sensors in the 77 GHz frequency band," *IEEE Trans. Microw. Theory Techn.*, vol. 60, no. 3, pp. 845–860, Mar. 2012.

[28] H.-J. Zepernick and A. Finger, *Pseudo Random Signal Processing: Theory and Application*, Hoboken, NJ, USA: Wiley, 2005.

[29] J. Wolfmann, "Almost perfect autocorrelation sequences," *IEEE Transactions on Information Theory*, vol. 38, no. 4, pp. 1412–1418, Jul. 1992.

[30] A. Pott and S. P. Bradley, "Existence and nonexistence of almost-perfect autocorrelation sequences," *IEEE Trans. Inf. Theory*, vol. 41, no. 1, pp. 301–304, Jan. 1995.

[31] A. T. Tasheva, Z. N. Tasheva, and A. P. Milev, "Generalization of the self-shrinking generator in the galois field GF(Pn)," *Adv. in Artif. Intell.*, vol. 2011–2:10, Jan. 2011, Art. no. 464971.

[32] W. V. Thillo, P. Gioffr, V. Giannini, D. Guermandi, S. Brebels, and A. Bourdoux, "Almost perfect auto-correlation sequences for binary phase-modulated continuous wave radar," in *Proc. Eur. Radar Conf.*, Oct. 2013, pp. 491–494.

[33] E. W. Weisstein, "Totient Function." [Online]. Available: http://mathworld.wolfram.com/TotientFunction.html

[34] P. Z. Fan, N. Suehiro, N. Kuroyanagi, and X. M. Deng, "Class of binary sequences with zero correlation zone," *Electron. Lett.*, vol. 35, no. 10, pp. 777–779, May 1999.

[35] H. Haderer, R. Feger, C. Pfeffer, and A. Stelzer, "Millimeter-wave phase-coded CW MIMO radar using zero- and low-correlation-zone sequence sets," *IEEE Trans. Microw. Theory Techn.*, vol. 64, no. 12, pp. 4312–4323, Dec. 2016.

[36] B. Fassi, A. Djebbari, T. -Ahmed. A, and I. Dayoub, "A new class of binary zero correlation zone sequence sets," *IOSR J. Electron. Commun. Eng.*, vol. 5, no. 3, pp. 15–19, 2013.

[37] H. Krim and M. Viberg, "Two decades of array signal processing research: The parametric approach," *IEEE Signal Process. Mag.*, vol. 13, no. 4, pp. 67–94, Jul. 1996.

[38] C. Schmid, R. Feger, C. Pfeffer, and A. Stelzer, "Motion compensation and efficient array design for TDMA FMCW MIMO radar systems," in *Proc. 6th Eur. Conf. Antennas Propag.*, Mar. 2012, pp. 1746–1750.

Jeroen Overdevest was born in 's-Gravenhage, The Netherlands, in 1993. He received the B.Sc. and M.Sc. degrees in electrical engineering from the Delft University of Technology, Delft, The Netherlands, in 2015 and 2018, respectively. After pursuing the M.Sc. thesis at NXP Semiconductors N.V., he joined the Algorithms & Software Innovation group (BL ADAS R&D) of NXP semiconductors N.V., Eindhoven, The Netherlands, in 2018. His research interests include signal processing and waveform design for mm-wave automotive radar applications.

Feike Jansen was born in 1980 in Eindhoven, The Netherlands. He received the master of science (M.Sc.) degree in Electrical Engineering from the Technical University of Eindhoven, Eindhoven, The Netherlands in 2006. In 2006 he joined Philips N.V. as a Researcher in the field of 24 GHz radar antennas. In 2007 he joined NXP Semiconductors N.V. where he is currently working as a Principal Scientist in the Algorithms and Software Innovation group. There he worked on algorithm development for 60 GHz wireless communication basebands. Since several years he has been working on algorithms and system design for 79 GHz automotive radar systems.

Faruk Uysal (SM16) received the M.S. and Ph.D. degrees in electrical engineering from New York University (NYU), New York, NY, USA, in 2010 and 2016, respectively. During his study, he focused on signal separation techniques for dynamic clutter mitigation. From 2011 to 2014, he was a Staff Engineer with C&P Technologies, Inc., Closter, NJ, USA. He was a Radar Engineer with the Advanced Radar Research Center (ARRC), The University of Oklahoma, Norman, OK, USA, from 2014 to 2016, where he worked on the design and implementation of various projects of the Department of Defense (DoD) Agencies. In 2016, he joined the Microwave Sensing, Signals and Systems (MS3) Section, Faculty of Electrical Engineering, Mathematics, and Computer Science (EEMCS), Delft University of Technology, as an Assistant Professor. He is also an Affiliate Member of the Advanced Radar Research Center (ARRC), The University of Oklahoma. His current research interests include radar signal processing, waveform design, beamforming, radar image formation, clutter mitigation, cognitive radar, and distributed radar systems.

Alexander Yarovoy (F'15) graduated from the Kharkov State University, Ukraine, in 1984 with the Diploma with honor in radiophysics and electronics. He received the Candidate Phys. & Math. Sci. and Doctor Phys. & Math. Sci. degrees in radiophysics, in 1987 and 1994, respectively. In 1987, he joined the Department of Radiophysics at the Kharkov State University as a Researcher and became a Professor there, in 1997. From September 1994 through 1996 he was with Technical University of Ilmenau, Ilmenau, Germany as a Visiting Researcher. Since 1999, he is with the Delft University of Technology, Delft, the Netherlands. Since 2009, he leads there a Chair of Microwave Sensing, Systems and Signals. He has authored and coauthored more than 450 scientific or technical papers, four patents and fourteen book chapters. His main research interests are in high-resolution radar, microwave imaging and applied electromagnetics (in particular, UWB antennas). Prof. Yarovoy served as a Guest Editor for five special issues of the IEEE Transactions and other journals. Since 2011, he is an Associated Editor of the International *Journal of Microwave and Wireless Technologies*. He is the recipient of the European Microwave Week Radar Award for the paper that Best advances the state-of-the-art in radar technology, in 2001 (together with L.P. Ligthart and P. van Genderen) and 2012 (together with T. Savelyev). In 2010, together with D. Caratelli Prof. Yarovoy got the Best Paper Award of the Applied Computational Electromagnetic Society (ACES). He served as the Chair and TPC Chair of the 5th European Radar Conference (EuRAD08), Amsterdam, the Netherlands, as well as the Secretary of the 1st European Radar Conference (EuRAD04), Amsterdam, the Netherlands. He also served as the Co-Chair and TPC Chair of the Xth International Conference on GPR (GPR2004) in Delft, the Netherlands. In the period 2008 to 2017, he served as Director of the European Microwave Association (EuMA).